J Biomol NMR (2009) 44:139–155
DOI 10.1007/s10858-009-9321-3

ARTICLE

Measuring $^{13}C^{\beta}$ chemical shifts of invisible excited states in proteins by relaxation dispersion NMR spectroscopy

Patrik Lundström · Hong Lin · Lewis E. Kay

Received: 10 February 2009 / Accepted: 20 April 2009 / Published online: 16 May 2009

Abstract A labeling scheme is introduced that facilitates the measurement of accurate $^{13}C^{\beta}$ chemical shifts of invisible, excited states of proteins by relaxation dispersion NMR spectroscopy. The approach makes use of protein over-expression in a strain of *E. coli* in which the TCA cycle enzyme succinate dehydrogenase is knocked out, leading to the production of samples with high levels of ^{13}C enrichment (30–40%) at C^{β} side-chain carbon positions for 15 of the amino acids with little ^{13}C label at positions one bond removed ($\approx$5%). A pair of samples are produced using [1-^{13}C]-glucose/Na$H^{12}CO_3$ or [2-^{13}C]-glucose as carbon sources with isolated and enriched (>30%) $^{13}C^{\beta}$ positions for 11 and 4 residues, respectively. The efficacy of the labeling procedure is established by NMR spectroscopy. The utility of such samples for measurement of $^{13}C^{\beta}$ chemical shifts of invisible, excited states in exchange with visible, ground conformations is confirmed by relaxation dispersion studies of a protein–ligand binding exchange reaction in which the extracted chemical shift differences from dispersion profiles compare favorably with those obtained directly from measurements on ligand free and fully bound protein samples.

Keywords CPMG · $^{13}C^{\beta}$ Chemical shifts · Selective labeling · Chemical exchange · Excited protein states

P. Lundström
Molecular Biotechnology/IFM, Linköping University, 581 83 Linköping, Sweden

H. Lin
Molecular Structure & Function, The Hospital for Sick Children, 555 University Avenue, Toronto, ON M5G 1X8, Canada

L. E. Kay (✉)
Department of Medical Genetics, The University of Toronto, One King's College Circle, Toronto, ON M5S 1A8, Canada
e-mail: kay@pound.med.utoronto.ca

L. E. Kay
Department of Biochemistry, The University of Toronto, One King's College Circle, Toronto, ON M5S 1A8, Canada

L. E. Kay
Department of Chemistry, The University of Toronto, One King's College Circle, Toronto, ON M5S 1A8, Canada

Introduction

A central catalyst in the emergence of solution NMR spectroscopy as a valuable technique for studies of protein structure and dynamics has been the development of powerful and robust labeling methods (Goto et al. 1999; Kainosho et al. 2006; LeMaster 1990). By suitably enriching molecules with NMR active nuclei it becomes possible to selectively 'turn on' a certain set of spin interactions that report on molecular properties of interest, while removing others that would complicate the interpretation of experiments. Labeling methods ranging from uniform incorporation of ^{15}N and/or ^{13}C (Kay et al. 1990a, b; Montelione and Wagner 1990) to selective ^{15}N, ^{13}C, ^{2}H (Farmer and Venters 1999; Gardner and Kay 1998; Grzesiek et al. 1993) or selective ^{1}H enrichment (Goto et al. 1999) have emerged in the past several decades, along with clever experiments that exploit the labeling in studies of structure and dynamics (Sattler et al. 1999). For example, in applications involving structural studies, uniformly ^{15}N, ^{13}C labeled samples are frequently produced for measurement of large numbers of distance restraints in the form of NOEs that are resolved through the chemical shifts of ^{15}N and ^{13}C heteroatoms (Kay et al. 1990a, b; Zuiderweg et al. 1991). Studies of

complexes most often involve mixtures of labeled and unlabeled components so that signals from each can be separated (Gross et al. 2003; Ikura and Bax 1992) and in cases of supra-molecular systems one approach labels only methyl groups with ^{13}C,^{1}H in an otherwise ^{12}C,^{2}H background (Tugarinov and Kay 2004).

The success of spin relaxation studies also depends critically on the appropriate labeling scheme. In some applications such as those involving the study of protein backbone dynamics uniformly ^{15}N labeled samples are employed (Kay et al. 1989) since it is possible to record ^{15}N relaxation rates without complications from ^{15}N–^{15}N three-bond scalar couplings that have been measured to be 0.1–0.4 Hz in proteins (Löhr and Rüterjans 1998). In contrast, homonuclear couplings can be very deleterious to the accurate measurement of ^{13}C transverse relaxation rates because such one-bond couplings are large, ranging between 35 and 60 Hz in proteins (Bystrov 1976), and because many of the classic approaches for measuring transverse relaxation involve the application of pulse trains that can lead to the undesired transfer of magnetization among homonuclear coupled spins, depending on the pulse rate (Ishima and Torchia 2003; Lundström et al. 2009; Mulder et al. 2002).

Despite the difficulties associated with the measurement of transverse relaxation rates, there is a strong incentive to do so. For example, in one class of experiment—the Carr-Purcell-Meiboom-Gill (CPMG) relaxation dispersion approach (Carr and Purcell 1954; Meiboom and Gill 1958)—protein motions can be probed on the milli-second (ms) time-scale, a regime that is frequently of relevance for a wide-range of biological processes. Here the transverse relaxation rate, $R_{2,\mathrm{eff}}$, of a nuclear spin is monitored as a function of the repetition rate of 180° refocusing pulses, ν_{CPMG} (Loria et al. 1999; Tollinger et al. 2001). In the simple case where the ms dynamics correspond to an exchange event between a pair of states $\mathrm{A} \underset{k_{\mathrm{BA}}}{\overset{k_{\mathrm{AB}}}{\longleftrightarrow}} \mathrm{B}$, and where the minor state B is populated to at least 0.5%, the $R_{2,\mathrm{eff}}$ (ν_{CPMG}) profile can be fitted to extract k_{AB}, k_{BA} (or equivalently the population of the excited state, p_{B}, and the exchange rate constant $k_{\mathrm{ex}} = k_{\mathrm{AB}} + k_{\mathrm{BA}}$) as well as the magnitude of the chemical shift differences between states A and B (Palmer et al. 2001, 2005). One of the major strengths of the method is that insight into the exchange process is obtained even in cases where the minor state is not observable in NMR spectra or for that matter by other biophysical techniques. The rate constants and populations determined by the relaxation dispersion method have provided valuable insights into the kinetics and thermodynamics of processes such as protein folding (Hill et al. 2000; Korzhnev et al. 2004; Sugase et al. 2007; Zeeb and Balbach 2005), enzyme catalysis (Boehr et al. 2006; Eisenmesser et al. 2002; Eisenmesser et al. 2005; Vallurupalli and Kay 2006; Watt et al. 2007; Wolf-Watz et al. 2004) and ligand binding (Mulder et al. 2001a, b; Sugase et al. 2007). The chemical shifts of the excited states are also very useful since they encode structural information (Spera and Bax 1991; Wishart and Case 2002; Wishart and Sykes 1994) that is, of course, not available from more conventional NMR approaches in cases where these excited states are below the level of direct detection.

To date the chemical shifts of backbone $^{13}C^{\alpha}$, ^{13}CO, ^{15}N, $^{1}H^{N}$ and $^{1}H^{\alpha}$ nuclei in invisible, excited states of proteins have been measured by relaxation dispersion NMR experiments (Hansen et al. 2008a, b; Ishima et al. 2004; Ishima and Torchia 2003; Korzhnev et al. 2005; Loria et al. 1999; Lundström et al. 2008, 2009) that, in some cases, have relied upon the development of novel labeling schemes to minimize the effects of homonuclear scalar couplings (Lundström et al. 2007a, b; 2009). The chemical shift restraints can be supplemented by additional restraints of the excited state that are provided through the orientation of bond vectors, measured via spin-state selective relaxation dispersion profiles recorded under conditions of fractional alignment (Igumenova et al. 2007; Vallurupalli et al. 2007). Recently the structure of an invisible state corresponding to a peptide bound form of the Abp1p SH3 domain was reported using restraints that were exclusively derived from relaxation dispersion data (Vallurupalli et al. 2008a, b) including $^{13}C^{\alpha}$, ^{13}CO, ^{15}N and $^{1}H^{N}$ chemical shifts (Vallurupalli et al. 2008a, b), $^{1}H^{N}$–^{15}N, $^{1}H^{N}$–^{13}CO, $^{1}H^{\alpha}$–$^{13}C^{\alpha}$ residual dipolar couplings (Hansen et al. 2008a, b; Vallurupalli et al. 2007) and residual ^{13}CO chemical shift anisotropies (Vallurupalli et al. 2008a, b).

It is clear that current relaxation dispersion methods offer a unique avenue for the investigation of excited states that are recalcitrant to study by most biophysical approaches. Additional probes of structure would, of course, also be of benefit. Although the chemical shift of $^{13}C^{\beta}$ is a sensitive indicator of secondary structure (Shen and Bax 2007; Spera and Bax 1991; Wishart and Sykes 1994), and a $^{13}C^{\beta}$ dispersion experiment would be a very useful addition to the growing array of dispersion methods that have been developed, such an experiment has not yet emerged. The major difficulty lies in the design of a suitable labeling scheme that results in high level enrichment of isolated $^{13}C^{\beta}$ spins. One approach, implemented by Palmer and coworkers (Lee et al. 1997; Wand et al. 1995) for ^{13}C relaxation studies of proteins, involves their expression using random, fractionally ^{13}C–labeled carbon sources. This strategy is problematic, however. Consider, for example, a C^{α}–C^{β}–C^{γ} fragment where the desired labeling places ^{13}C only at the C^{β} position. A carbon source that is 1/3 randomly enriched produces the maximum population of $^{12}C^{\alpha}$–$^{13}C^{\beta}$–^{12}C fragments (4/27), but undesired fragments with ^{13}C labeling at C^{β} and at least one of the other two

carbon positions are also generated (5/27), necessitating the use of some sort of purging scheme. This is certainly feasible (Mulder et al. 2002; Wand et al. 1995) but at the expense of considerable loss in sensitivity since the purging elements typically are on the order of $1/(2J_{CC}) \approx 15$ ms, where J_{CC} is the one-bond ^{13}C–^{13}C scalar coupling constant. A second approach, based on the work of LeMaster and Kushlan, involves over-expression of proteins in a modified *E. coli* strain with the appropriate ^{13}C-labeled precursors, leading to the production of the desired labeling profile (LeMaster and Kushlan 1996). Herein we build upon this strategy and develop a robust method for the production of proteins with selective $^{13}C^{\beta}$-labeling at a much higher enrichment level than is available from the fractional labeling approach discussed above. In the application considered here a pair of samples are produced by over-expression in a genetically modified bacterial strain using [1-^{13}C]-glucose/NaH$^{12}CO_3$ or [2-^{13}C]-glucose as carbon sources. We show that this method leads to nearly isolated $^{13}C^{\beta}$ enrichment for 15 residue types at levels of ^{13}C incorporation between 30 and 40%. It is demonstrated that accurate $^{13}C^{\beta}$ chemical shifts of invisible, excited states can be obtained from dispersions measured in proteins labeled in this manner using pulse schemes that do not include any purging elements.

Materials and methods

Generation of the bacterial strain BL21(DE3)Δ*sdh*

The *sdh* operon, consisting of genes *sdhC*, *sdhD*, *sdhA* and *sdhB*, was knocked out from *BL21*(*DE3*) cells by replacing it with a frt-flanked (see below) kanamycin resistance (Km^R) expression cassette by Red mediated homologous recombination (Datsenko and Wanner 2000). The Km^R gene was amplified from the plasmid pKD4 (Datsenko and Wanner 2000) by PCR using primers designed to provide 50 bp sequence homology to regions upstream, (*cccgacgtctccaggtaacagaaagttaacctctgtgcccgtagtccccagtgtaggctggagctgcttc*) and downstream (*ccggcactggttgcctgatgcgacgcttgcgcgtcttatcaggcctacggcatatgaatatcctccttag*) of the *sdh* operon, respectively. *BL21*(*DE3*) cells were initially transformed with the plasmid pKD46 that encodes λ Red proteins (γ, β, *exo*) under control of an L-arabinose inducible promoter and that carries a temperature sensitive origin of replication (Datsenko and Wanner 2000). After induction with L-arabinose (that produces the λ proteins for recombination), the Km^R PCR fragment was introduced to the cells by electroporation and these cells were subsequently grown for 3 h at 37°C. During this time incorporation of the Km^R gene into the *E. coli* genome occurs, while the increased temperature ensures that pKD46 no longer replicates. Selection of those cells with the Km^R gene is achieved by plating on LB-agar plates containing 15 μg/ml kanamycin. Colonies were screened for homologous recombination by PCR using the primer, *cccagcgttgtaacgtgtcg*, that binds upstream of the targeting construct and the internal primer, *catatgaatatcatccttag* (Datsenko and Wanner 2000); a specific PCR product of 1,634 bp is obtained only in the case of homologous recombination while no PCR product is obtained in the case the Km^R gene has integrated into the wrong location. PCR products were sequenced to verify that they did not result from nonspecific priming in the PCR reactions.

Protein samples

Two different isotopically enriched samples of the Abp1p SH3 domain (Drubin et al. 1990; Lila and Drubin 1997; Rath and Davidson 2000) were prepared by protein over-expression in *BL21*(*DE3*)Δ*sdh* cells using M9 medium with 1 g/L $^{15}NH_4Cl$ and 3 g/L of either [1-^{13}C]-glucose or [2-^{13}C]-glucose as nitrogen and carbon sources, respectively. The growth with [1-^{13}C]-glucose was supplemented with 20 mM NaH$^{12}CO_3$ at the start, with an additional 10 mM at the time of induction. Cells were grown to OD = 0.8 and protein expression was induced with 1 mM IPTG. Protein expression was carried out overnight at room temperature for the [1-^{13}C]-glucose culture and at 37°C for 4 h for the [2-^{13}C]-glucose culture; neither of the samples had significant differences in levels of $^{13}C^{\beta}$ labeling for the subset of residues that were expected to be enriched from each carbon source, suggesting, at least in this application, that the labeling pattern is relatively insensitive to the length of expression. Purification of the Abp1p SH3 domain as well as an unlabeled 17 residue peptide from Ark1p (Haynes et al. 2007) (primary sequence: KKTKPTPPP KPSHLKPK) was performed as previously described (Vallurupalli et al. 2007). Proteins were prepared in a buffer comprised of 50 mM sodium phosphate, 100 mM NaCl, 1 mM EDTA, 2 mM NaN_3, pH 7.0. The solvent was 100% D_2O for the relaxation experiments and 10% D_2O/90% H_2O for analysis of incorporation of label at C^{β} and for the titration of Ark1p peptide. The protein concentrations were approximately 1 mM.

NMR spectroscopy

All NMR experiments were performed at 25°C on Varian Inova spectrometers with ^1H resonance frequencies of 500, 600 and 800 MHz, equipped with cryogenically cooled (600 MHz) and room temperature (500, 800 MHz) probeheads.

Analysis of incorporation of ^{13}C label at the C^{β} position was performed by comparison of peak intensities of

selectively and uniformly ^{15}N,^{13}C labeled samples in non-constant time ^{13}C–^{1}H correlation maps. To compensate for different sample concentrations, the intensities were normalized with the average intensities of correlations in ^{15}N–^{1}H correlation maps and the fractional ^{13}C enrichment at C^{β} was calculated as $f = (C_s/\bar{N}_s)/(C_u/\bar{N}_u)$, in which C_s and C_u are the intensities of a particular $^{13}C^{\beta}$–$^{1}H^{\beta}$ correlation in the selectively and uniformly labeled samples respectively and $\bar{N}_s$and $\bar{N}_u$ are the average intensities of ^{15}N–^{1}H correlations in each of the two samples compared. Note that the peaks were integrated in a way so that values of f include contributions from $^{13}C^{\beta}$–^{13}C fragments. ^{13}C–^{1}H correlation spectra were also used to evaluate the fraction of isolated ^{13}C label at the C^{β} position for each residue, by measuring the volumes of correlations comprising the central C^{β} component as well as of the multiplet components that arise from one-bond $^{13}C^{\beta}$–^{13}C couplings.

Samples containing the Abp1p SH3 domain and the Ark1p peptide were prepared by titration. The mole fraction of bound protein, p_B, was established by recording ^{15}N relaxation dispersion profiles of the protein. Complexes with $p_B \approx 12\%$ ([1-^{13}C]-glucose) and $\approx 4\%$ ([2-^{13}C]-glucose) were generated and used for subsequent analyses.

$^{13}C^{\beta}$ relaxation dispersion profiles for residue types with $C^{\beta}H_2$ groups were measured as described in the text for the samples listed above. Data sets were recorded at both 600 and 800 MHz using T_{relax} values of either 20 or 30 ms. An even number of refocusing pulses was applied during $T_{relax}/2$ with ν_{CPMG} values (defined as $\nu_{CPMG} = 1/(4\tau_{cp})$ where $2\tau_{cp}$ is the separation between successive refocusing pulses) within the range 67–1,000 Hz. Each complete dispersion set at one static magnetic field was recorded in approximately 20 h. For the sample prepared with [1-^{13}C]-glucose, $p_B \approx 12\%$, $^{13}C^{\beta}$ relaxation dispersion profiles were also recorded for Ala ($C^{\beta}H_3$) and Thr ($C^{\beta}H$), using previously published pulse sequences designed for methyl group and $^{13}C^{\alpha}$ probes, respectively (Hansen et al. 2008b; Lundström et al. 2007b). Data sets were processed with nmrPipe (Delaglio et al. 1995) and peaks were integrated using the program FuDA (http://pound.med.utoronto.ca/software.html). Effective transverse relaxation rates were calculated using the relation $R_{2,eff}(\nu_{CPMG}) = -\ln(I(\nu_{CPMG})/I_0)/T_{relax}$, where $I(\nu_{CPMG})$ and I_0 are peak intensities from spectra recorded with and without the CPMG block (Tollinger et al. 2001). Uncertainties in $R_{2,eff}$ were estimated from duplicate experiments.

The resulting CPMG dispersion profiles were fitted to a two-state exchange process for which the fitting parameters include the global exchange rate, k_{ex}, and the population of the minor state, p_B, as well as residue specific parameters such as chemical shift differences between spin probes in the major and minor states (absolute values only), $|\Delta\varpi|$, and residue specific exchange-free contributions to relaxation, $R_{2,0}$. In order to establish which residues should be included in such fits, all dispersion profiles were initially fit on a per-residue basis to models that either include or do not include chemical exchange. Residues were retained for further analysis if fits using the two-site exchange model were significant as established by F-test analyses (Press et al. 1988) with $p < 0.001$ and if the magnitude of the dispersion profile measured at 800 MHz, $\Delta R_{2,eff} = R_{2,eff}(\nu_{CPMG} = 100\,Hz) - R_{2,eff}(\nu_{CPMG} = \infty) \geq 5\ s^{-1}$. The latter constraint was included to eliminate artifactual dispersion profiles with small $\Delta R_{2,eff}$ values ($<2\ s^{-1}$) that derive from $^{13}C^{\beta}$–^{13}C couplings and to ensure that the contributions from such artifacts to dispersion profiles that are retained for analysis are small.

Results and discussion

The design of a labeling scheme producing isolated $^{13}C^{\beta}$ spins

A major challenge in applications involving ^{13}C transverse relaxation measurements in proteins derives from large homonuclear one-bond ^{13}C–^{13}C scalar couplings that typically range from approximately 35–60 Hz (Bystrov 1976). These couplings modulate echo amplitudes in CPMG based experiments, so that signal intensities become a function not only of transverse relaxation rates but also reflect potentially complex pathways of coupling evolution (Freeman 1999; Hahn and Maxwell 1952). It is clear, therefore, that selective labeling schemes must be developed that produce a high level of ^{13}C enrichment at the desired positions but not at adjacent carbons. In this regard a particularly elegant approach has been suggested by LeMaster and Kushlan (1996) involving protein overexpression in a strain of *E. coli* lacking both succinate (*sdh*) and malate dehydrogenase (*mdh*), two TCA cycle enzymes. Selective ^{13}C enrichment of the protein thioredoxin was achieved through expression with either [2-^{13}C]-glycerol, $NaH^{13}CO_3$ or [1,3-^{13}C]-glycerol, $NaH^{12}CO_3$ that produced isolated ^{13}C spins for most of the amino acids. Although this approach is, in principle, very powerful for generating isolated $^{13}C^{\beta}$ label we were not successful in expressing proteins of interest to us using the bacterial strain lacking these two enzymes. Part of the problem may reflect the fact that protein production using an IPTG inducible T7 RNA polymerase, that has become the standard for high level protein expression, is not possible using this strain since the *DE3* gene is lacking (Studier and Moffatt 1986). Rather over-expression is achieved via heat induction (42°C) and bacterial growth can often be slow at higher temperatures. A second concern was that perhaps with two enzymes deleted the cells were less able to generate large quantities

of protein in general. It is of interest to note in this context that the LeMaster/Kushlan labeling scheme (i.e., growth on 1,3- or 2-^{13}C glycerol) has found important applications in solid-state NMR structural studies (Castellani et al. 2002; Wasmer et al. 2008), but to our knowledge in all cases expression is carried out in cell lines that do not lack either of the *sdh* and *mdh* genes.

With these problems in mind we sought a more 'mild' knockout strategy that would (1) allow high levels of protein expression in the commonly used *BL21(DE3)* cell line, (2) allow the production of high levels of protein using glucose as the carbon source since our experience has been that many proteins are expressed to much higher yields when glucose is used and (3) lead to high levels of isolated or near isolated $^{13}C^{\beta}$ spins.

Insight into how this might be achieved can be obtained by studying glycolysis and the TCA cycle (Voet and Voet 1995), the main metabolic pathways involved in the biosynthesis of 18 of the 19 relevant amino acids for the applications considered here. We first consider the intact pathways to illustrate why a knockout strategy is essential in this case, Fig. 1. The ultimate precursor of C^{β} for many residues is position 1 (or equivalently position 6) of glucose and it is reasonable, therefore, to consider a strategy of labeling of amino acids starting from [1-^{13}C]-glucose as the carbon source. It is readily apparent that the amino acids derived from the glycolytic intermediates 3-phosphoglycerate (3PG), phosphoenolpyruvate (PEP) and pyruvate (Ala, Cys, Lys, Phe, Ser, Trp, Tyr) will be enriched in ^{13}C at C^{β} but not at C^{α} or C^{γ}. Asn, Asp, Lys, Met and Thr, which are derived from oxaloacetate (OA), will also be ^{13}C enriched at C^{β} and not at other carbon sites if OA is formed by carboxylation of PEP. However, there are a number of complicating factors associated with the production of these residues. First, a significant amount of $^{13}CO_2$ is produced by both the TCA cycle and the pentose phosphate pathway, that also is a source for amino acids (Voet and Voet 1995), when [1-^{13}C]-glucose is used as the carbon source, leading to a substantial population of OA derived residues with $^{13}C^{\beta}$–$^{13}C^{\gamma}$ coupled pairs. A partial remedy is to dilute the $^{13}CO_2$ by addition of $NaH^{12}CO_3$ to the growth medium (LeMaster and Kushlan 1996). Second, OA is regenerated by the TCA cycle, produced from malate that is either ^{13}C labeled at the 1,3 or 2,4 positions (Fig. 1, 'First Pass'). This leads to a dilution of the desired label after the first round and to the production of amino acids with isolated $^{13}C^{\beta}$ in successive rounds in the case that the starting precursor is 1,3 labeled OA. However, if the starting precursor is 2,4-^{13}C OA then Asn, Asp, Lys, Met and Thr are produced with undesired $^{13}C^{\beta}$–$^{13}C^{\alpha}$ spin-pairs (see Fig. 1, 'Second Pass'). Similar problems emerge with Arg, Glu, Gln and Pro, precursors of the TCA intermediate α-ketoglutarate (AKG). Starting from OA labeled with ^{13}C at the 3 position ('First Pass' of the TCA cycle) the AKG derived residues are not labeled at the C^{β} position but subsequent passes through the cycle using newly synthesized 2,4-^{13}C OA can produce residues that are labeled with ^{13}C at both C^{β} and C^{γ} positions (Fig. 1, 'Second Pass'). Unfortunately, the high flux through the TCA cycle in bacteria grown aerobically ensures that an unacceptably high fraction of $^{13}C^{\beta}$ will be present in the form of ^{13}C–^{13}C spin-pairs, leading to complications in transverse relaxation experiments.

A potential solution to these problems would be achieved by blocking the TCA cycle after the production of AKG so that OA is produced exclusively from carboxylation of PEP. This would minimize both dilution of label and the formation of $^{13}C^{\beta}$–^{13}C spin-pairs described above, leading to the production of 11 amino acids (derived from 3PG, PEP, pyruvate and OA) with (near) isolated $^{13}C^{\beta}$ positions if [1-^{13}C]-glucose and $NaH^{12}CO_3$ are used as carbon sources. Conversely, the desired labeling for residues derived from AKG (Arg, Glu, Gln and Pro) is obtained using [2-^{13}C]-glucose as the carbon source. In total, therefore, 15 amino acid residue types would be produced with isolated $^{13}C^{\beta}$ spins. This, of course, is similar to the approach of LeMaster and Kushlan (LeMaster and Kushlan 1996) described above, but as we show below only a single enzyme need be eliminated, that in our hands produces much more robust over-expression of protein.

With this in mind an *E. coli* strain, *BL21(DE3)*Δ*sdh*, was designed following the method of Datsenko and Wanner (Datsenko and Wanner 2000) that has the entire succinate dehydrogenase (*sdh*) operon, comprised of the genes (*sdhC*, *sdhD*, *sdhA* and *sdhB*), replaced by a kanamycin resistance (Km^R) expression cassette. The basis for choosing *sdh* as the target of the knockout is that it catalyzes a rather late step in the TCA cycle, importantly after AKG is formed, and that no other enzymes catalyze the dehydrogenation of succinate. By contrast, there are at least two genes for malate dehydrogenase (Cronan and LaPorte 1996; Molenaar et al. 1998). *BL21(DE3)* was chosen as the parental strain because of its well documented suitability for protein expression. We used an Km^R cassette that is flanked by frt-sites (Datsenko and Wanner 2000) that are recognized by flp recombinase (Gronostajski and Sadowski 1985) so that it can be excised by transforming the *BL21(DE3)*Δ*sdh* cells with a plasmid encoding flp, for instance pCP20 (Datsenko and Wanner 2000). However, we prefer to leave the selection marker intact since it can then be used to select against contamination by wild-type cells. The *BL21(DE3)*Δ*sdh* strain was found to grow well on M9 medium at least when glucose was used as the carbon source and to give good levels of over-expression of recombinant proteins under these conditions. Indeed, the

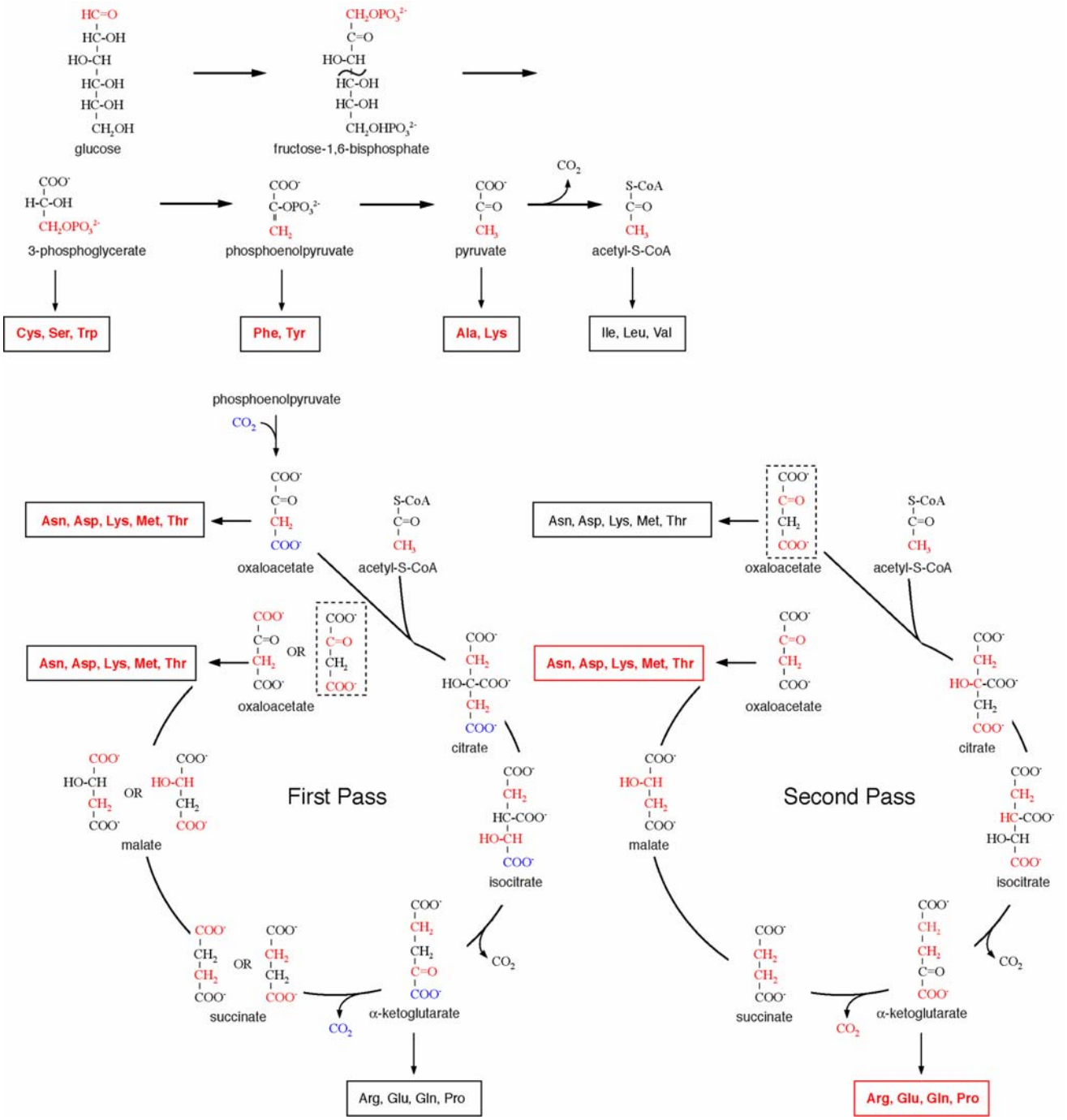

Fig. 1 Major metabolic pathways involved in the production of amino acids, including key steps in glycolysis and two subsequent rounds of the TCA cycle, focusing on ^{13}C labeling at the C^{β} position. Intermediates in glycolysis and in the TCA cycle are precursors for C^{β} in 18 of the 19 relevant amino acids (His is the only exception). Positions highlighted in *red* will be ^{13}C enriched if [1-^{13}C]-glucose is the carbon source during growth whereas positions that are enriched due to the presence of $^{13}CO_2$ in the growth medium are shown in *blue*. Amino acids derived from the different intermediates are shown within boxes; residues indicated in *red* are those enriched in ^{13}C at C^{β} with the *black or red frames* delineating residues for which isolated $^{13}C^{\beta}$ (*black*) or $^{13}C^{\beta}$–^{13}C pairs (*red*) are produced. Residues indicated in *black* are not labeled with ^{13}C at C^{β}. Oxaloacetate (OA) produced by carboxylation of PEP is used as a substrate in the first round of the TCA cycle, producing OA with a pair of different labeling schemes as products. The two different labeling patterns derive from the fact that the TCA cycle intermediate succinate is symmetric so the subsequent TCA cycle intermediates may be labeled in two different ways. OA shown in the *dashed box* is used as input into a second pass of the TCA cycle to illustrate how α-ketoglutarate (AKG) derived amino acids can be produced with ^{13}C labeling at both C^{β} and C^{γ} positions. Note that C^{β} of Lys can be derived from either pyruvate or oxaloacetate due to a symmetric intermediate in its biosynthesis (Voet and Voet 1995)

level of protein expression was found to be only 25% lower than what is obtained from growths in *BL21*(*DE3*) cells. Reasonable yields of protein were obtained with glycerol as the sole carbon source as well (although lower than for expression with glucose). Tests established that at least 20 mM $NaHCO_3$ could be added to M9 medium without slowing the growth of this strain.

The modified metabolic pathways and the expected labeling patterns of amino acids in proteins produced from expression in *BL21*(*DE3*)Δ*sdh* cells using [1-^{13}C]-glucose/$NaH^{12}CO_3$ are shown in Fig. 2a. Residues indicated in red and surrounded by black boxes are those for which (near) isolated $^{13}C^{\beta}$ spins are obtained (see below). Residues in black are those that are unlabeled at C^{β} using these precursors, while residues highlighted in red and surrounded with a red box are those for which a high fraction of $^{13}C^{\beta}$–^{13}C spin-pairs is anticipated (and observed in experiment, see below), based on the labeling patterns of precursor molecules. A potential issue of concern in connection with the production of amino acids with isolated $^{13}C^{\beta}$ spins is that the TCA cycle can be short circuited by the glyoxylate shunt, in which isocitrate is cleaved into glyoxylate and succinate, Fig. 2a. Glyoxylate may subsequently combine with Ac–S–CoA to yield malate and ultimately oxaloacetate, which as depicted in Fig. 2a may be simultaneously labeled at positions 2 and 3 that become C^{α} and C^{β} in residues derived from it. In addition, OA labeled in this manner can reenter the TCA cycle to produce ^{13}C labeling of the AKG derived residues at C^{α}, C^{β} and C^{γ}. This is particularly troubling since the glyoxylate shunt is up-regulated in certain E. *coli* strains deficient in *sdh* (Li et al. 2006), however, as we show below, this is less problematic than anticipated and ≥93% of the $^{13}C^{\beta}$ spins in the relevant amino acids are isolated.

Figure 2b illustrates that the AKG derived residues, Arg, Gln, Glu and Pro, can be labeled at C^{β} in proteins overexpressed in *BL21*(*DE3*)Δ*sdh* cells using [2-^{13}C]-glucose as the carbon source. In this case the glyoxylate shunt does not produce $^{13}C^{\beta}$–^{13}C spin-pairs although it does lead to reduced incorporation of ^{13}C at C^{β}. Residues Ile, Leu and Val are very significantly labeled at the β position (≈45%), with equal mixtures of $^{12}C^{\alpha}$–$^{13}C^{\beta}$, $^{13}C^{\alpha}$–$^{13}C^{\beta}$ (Ile, Val) or $^{12}C^{\gamma}$–$^{13}C^{\beta}$, $^{13}C^{\gamma}$–$^{13}C^{\beta}$ (Leu) fragments produced; measurement of accurate $^{13}C^{\beta}$ transverse relaxation rates for these residues is predicated on eliminating magnetization derived from $^{13}C^{\beta}$–^{13}C spin-pairs. The biosynthesis of Val is shown at the bottom of Fig. 2b, illustrating how label at both C^{α} and C^{β} emerges (similar scenarios pertain for Ile and Leu). Finally, His is not labeled at C^{β} using either of these carbon sources since it is ultimately derived from position 4 of glucose.

Incorporation of ^{13}C label at C^{β}

If the only active pathways in the production of amino acids are glycolysis and the interrupted TCA cycle shown in Fig. 2 then the level of ^{13}C incorporation at C^{β} positions (that includes both isolated and non-isolated label) is predicted to be 50% (with the exception of His, see above). This upper bound derives from the fact that glucose is split into two molecules of 3PG, only one of which is labeled at position 3 in the case of [1-^{13}C]-glucose and at position 2 in the case of [2-^{13}C]-glucose. In order to quantify the actual level of incorporation, signal intensities in ^{13}C–^{1}H correlation spectra of selectively ^{13}C labeled samples of the Abp1p SH3 domain prepared using either [1-^{13}C]-glucose or [2-^{13}C]-glucose were compared with the corresponding correlations in a uniformly ^{15}N,^{13}C labeled sample. Differences in sample concentrations were accounted for by normalizing according to the average peak intensities in ^{15}N–^{1}H correlation maps, as described in the section 'Materials and methods'. The percentage enrichment for each residue is listed in Table 1. Using [1-^{13}C]-glucose as the precursor the fractional incorporation of $^{13}C^{\beta}$ is rather uniform, with values of 33–43% for all amino acids that are predicted to be ^{13}C enriched at the C^{β} position, slightly lower than the expected 50%. The smaller than predicted values are not likely the result of the glyoxylate shunt since the OA formed via this pathway is also 50% ^{13}C labeled at C^{β}. Rather, they likely reflect the operation of the pentose phosphate pathway that generates unlabeled intermediates from [1-^{13}C]-glucose (Voet and Voet 1995). Small levels of enrichment (5%) were noted at the β-positions of AKG derived residues, resulting from 2,3 ^{13}C labeled OA produced from the glyoxylate shunt that subsequently enters the TCA cycle, Fig. 2a, discussed above. As expected, we did not detect any $^{13}C^{\beta}$ enrichment for Ile, Leu and Val.

Amino acids in the Abp1p SH3 domain produced from [2-^{13}C]-glucose that are predicted to be highly enriched at $^{13}C^{\beta}$ (Gln, Glu, Ile, Leu, Pro, Val) were found to have levels of incorporation ranging from 29–46% (although some are not isolated). Here the glyoxylate shunt does not lead to $^{13}C^{\beta}$ labeling but the pentose phosphate pathway can (Voet and Voet 1995), accounting for the small levels of enrichment in residues that are not predicted to have $^{13}C^{\beta}$ label on the basis of glycolysis and the TCA cycle, Fig. 2b. Notably, some level of ^{13}C enrichment at the C^{β} position was detected for all residue types present in the Abp1p SH3 domain produced using the [2-^{13}C]-glucose precursor. Residues derived from OA were labeled to ≈ 10% as were those produced from 3PG, while Phe and Tyr, derived from PEP, were $^{13}C^{\beta}$ enriched to approximately 5%. Finally, it is worth noting that the fractional ^{13}C incorporation at the C^{β} position for residues types that either are not present in the

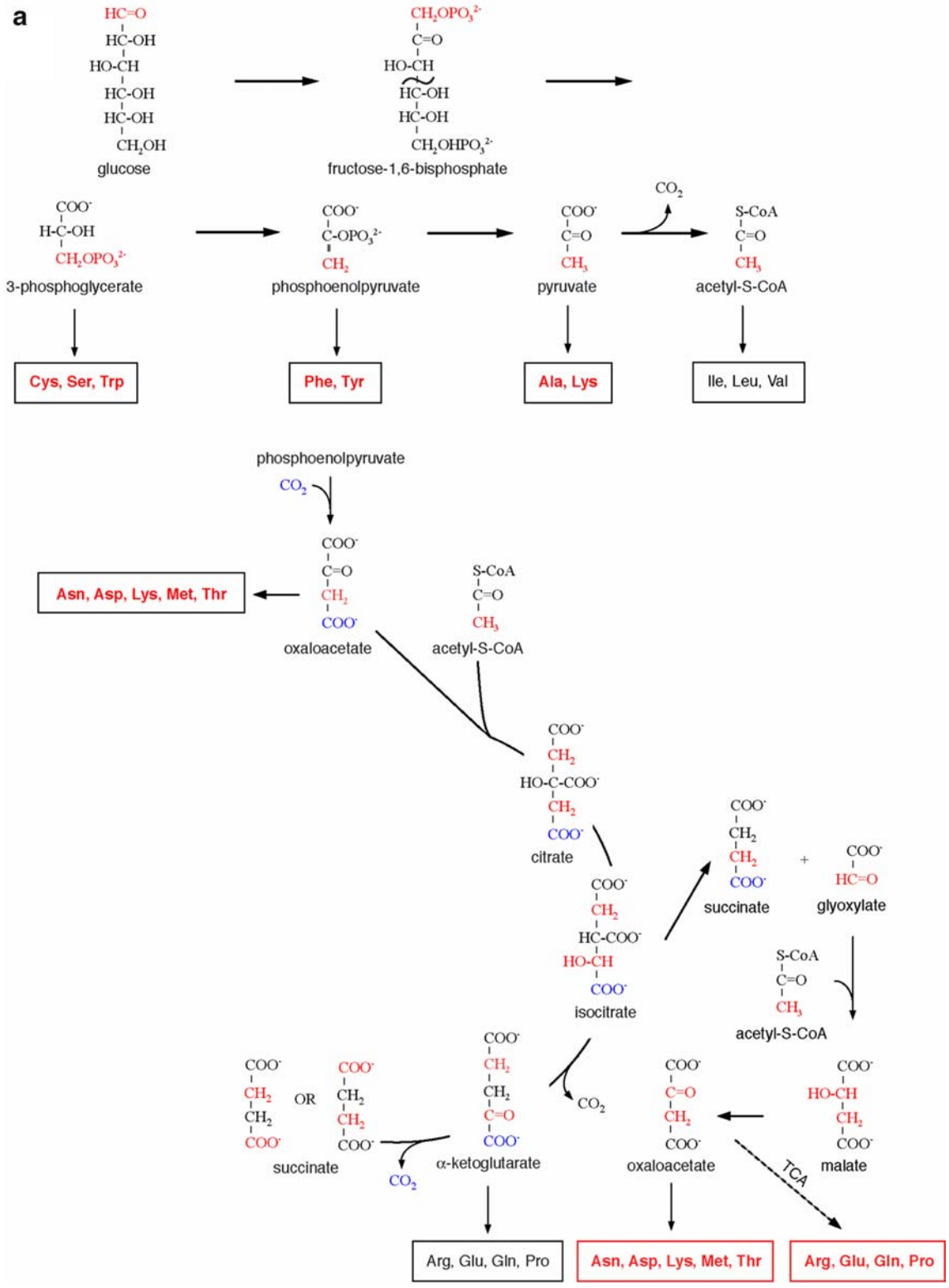

Fig. 2 Biosynthetic pathways involved in ^{13}C labeling at the C^{β} positions of amino acids in bacteria deficient in succinate dehydrogenase, e.g. *BL21(DE3)Δsdh*, showing glycolysis, the interrupted TCA cycle and the glyoxylate shunt. See legend of Fig. 1 for more details. Expected labeling patterns if [1-^{13}C]-glucose **a** or [2-^{13}C]-glucose **b** is used as the carbon source are indicated. Also shown is the biosynthesis and expected labeling pattern of the hydrophobic amino acid Val. The hydroxyethyl group of hydroxyethyl-TPP participating in the first step is an intermediate in the formation of Ac–S–CoA (Voet and Voet 1995)

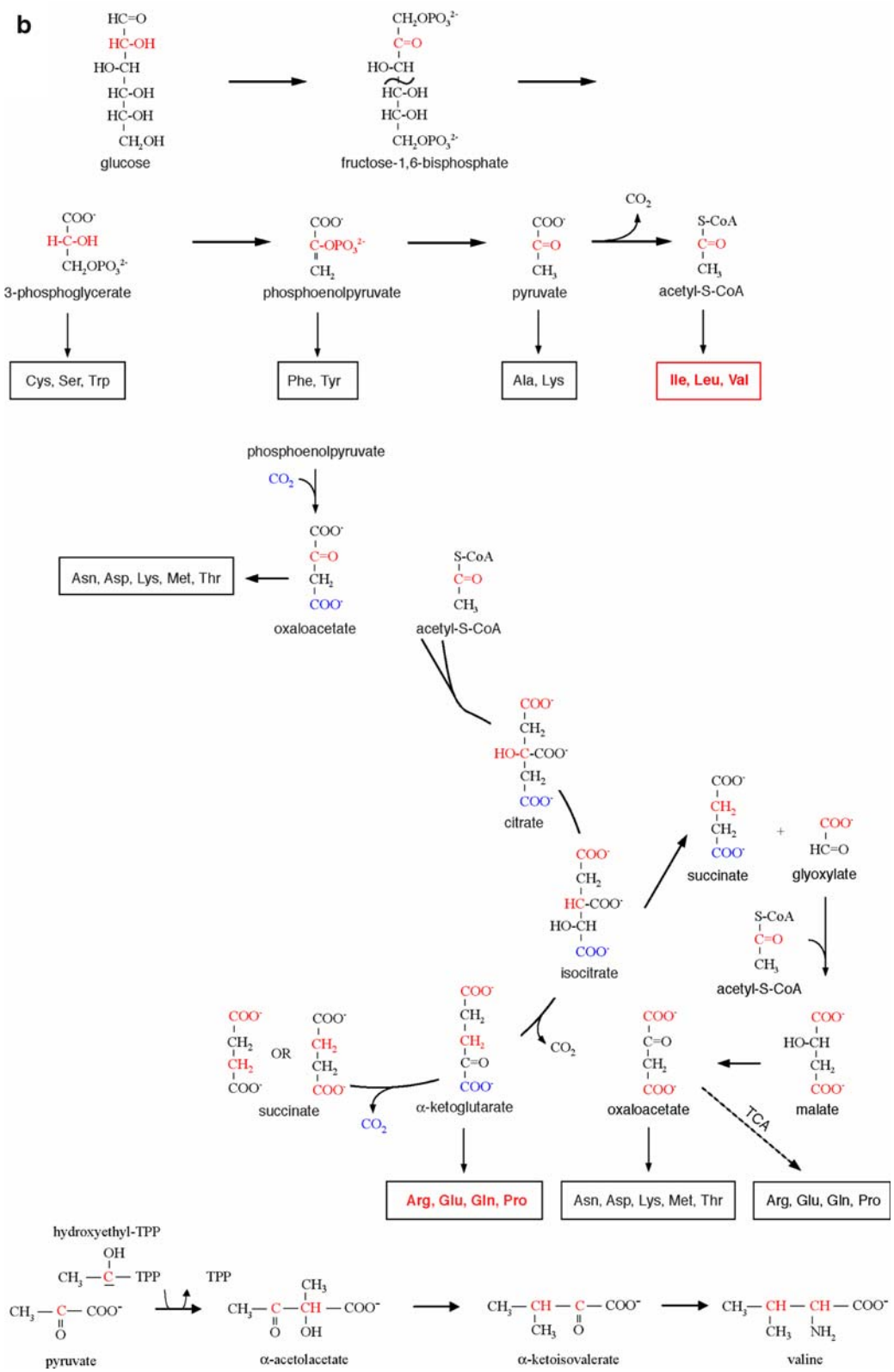

Fig. 2 continued

Table 1 Fractional ^{13}C enrichment at C^{β} and the fraction of isolated $^{13}C^{\beta}$ positions for different amino acid residue types produced by over-expression in *BL21(DE3)*Δ*sdh* cells using the indicated carbon sources

Amino acid	[1-^{13}C]-glucose/NaH$^{12}CO_3$		[2-^{13}C]-glucose	
	Total enrichment	Fraction isolated[a]	Total enrichment	Fraction isolated[a]
Ala	**0.41 ± 0.002 (2)**	**0.94 ± n.a. (1)**	0.09 ± 0.008(2)	0.89 ± 0.05 (2)
Arg[b]	n.a.	0.66 ± 0.04 (2)[c]	**n.a.**	**0.95 ± 0.02 (4)**[c]
Asn	**0.33 ± 0.04 (3)**	**0.93 ± 0.02 (3)**	0.11 ± 0.02 (3)	0.93 ± 0.02 (2)
Asp	**0.35 ± 0.007 (2)**	**0.93 ± 0.02 (3)**	0.12 ± 0.02 (2)	0.93 ± 0.02 (2)
Cys[b]	**n.a.**	**0.94 ± 0.05 (2)**[c]	n.a.	0.74 ± 0.01 (3)[c]
Gln[b]	n.a.	0.66 ± 0.04 (2)[c]	**n.a.**[a]	**0.95 ± 0.02 (4)**[c]
Glu	0.05 ± 0.01 (2)	0.66 ± 0.04 (2)	**0.39 ± 0.05 (2)**	**0.95 ± 0.02 (4)**
His[b, d]	n.a.	n.a.	n.a.	n.a.
Ile[e]	n.a.	n.a.	0.43 ± 0.04 (3)	0.55 ± 0.03 (3)
Leu[e]	n.a.	n.a.	0.42 ± 0.04 (4)	0.57 ± 0.05 (7)
Lys	**0.33 ± 0.05 (3)**	**0.97 ± 0.01 (3)**	0.11 ± 0.007 (3)	0.95 ± 0.03 (3)
Met[f]	**n.a.**	**0.93 ± 0.02 (3)**	n.a.	0.93 ± 0.02 (2)
Phe	**0.33 ± 0.0004 (2)**	**0.95 ± n.a. (1)**	0.04 ± 0.0008 (2)	0.58 ± 0.05 (3)
Pro	0.05 ± 0.006 (2)	0.66 ± 0.04 (2)	**0.29 ± 0.01 (2)**	**0.95 ± 0.02 (4)**
Ser	**0.43 ± 0.08 (3)**	**0.94 ± 0.05 (2)**	0.12 ± 0.01 (3)	0.74 ± 0.01 (3)
Thr	**0.34 ± 0.002 (2)**	**0.93 ± 0.02 (3)**	0.10 ± 0.009 (2)	0.93 ± 0.02 (2)
Trp	**0.35 ± 0.03 (2)**	**0.94 ± 0.05 (2)**	0.08 ± 0.02 (4)	0.74 ± 0.01 (3)
Tyr	**0.36 ± 0.02 (2)**	**0.95 ± n.a. (1)**	0.06 ± 0.003 (2)	0.58 ± 0.05 (3)
Val[e]	n.a.	n.a.	0.46 ± n.a. (1)	0.57 ± 0.05 (7)

[a] Residues highlighted in bold are those that can be used for measurement of $^{13}C^{\beta}$ relaxation dispersion profiles, with the labeling scheme described (i.e., sufficient levels of enrichment and isolation). Results for residues derived from the same precursor were averaged

[b] Not present in the Abp1p SH3 domain

[c] Expected fraction of isolated $^{13}C^{\beta}$ based on the results from amino acids produced from the same precursors

[d] His is not labeled at C^{β} with the glucose precursors used

[e] These residue types are not expected to be enriched using [1-^{13}C]-glucose as carbon source

[f] The ^{13}C enrichment at C^{β} could not be quantified due to spectral overlap in the spectrum of the uniformly ^{13}C labeled protein

Abp1p SH3 domain or that could not be quantified is expected to be very similar to values quantified for residues that are derived from the same precursor (*i.e.*, values for Met will be close to those for Asn, Asp, Lys and Thr).

It is clear from the above discussion (and Table 1) that quite high levels of $^{13}C^{\beta}$ label can be generated using [1-^{13}C]- and [2-^{13}C]-glucose precursors. This is necessary but not sufficient for applications involving ^{13}C transverse relaxation measurements since a prerequisite is also that the labeling scheme produce minimal levels of $^{13}C^{\alpha}$–$^{13}C^{\beta}$ and $^{13}C^{\beta}$–$^{13}C^{\gamma}$ fragments. To analyze whether in fact this is the case ^{13}C–^{1}H correlation spectra were recorded with high resolution in the ^{13}C dimension (acquisition times of 90 ms in t_1). Isolated ^{13}C enriched positions appear as singlets whereas doublets separated by 35–55 Hz indicate a ^{13}C–^{13}C spin-pair; more complex multiplet patterns were not observed. Figure 3 shows F_1 traces through $^{13}C^{\beta}$–$^{1}H^{\beta}$ correlations of all amino acid types present in the Abp1p SH3 domain produced using either [1-^{13}C]- (a) or [2-^{13}C]-glucose (b). The traces have been scaled to reflect the level of fractional enrichment in the singlet component (Total Enrichment x Fraction Isolated, as reported in Table 1). For the sample produced with [1-^{13}C]-glucose/NaH$^{12}CO_3$ it is clear that almost all of the intensity of the correlations derive from the singlet component, with a very small but measurable doublet seen in most cases (each multiplet component of the doublet corresponds to less than 3.5% of the total signal, Table 1). The ratios of peak volumes of the singlet (V_S) and singlet + doublet ($V_S + V_D$) components that have been quantified in 2D correlation maps, $V_S/(V_S + V_D)$, are listed in Table 1 (under Fraction Isolated); all values for the 11 amino acids that are suitably labeled from [1-^{13}C]-glucose/NaH$^{12}CO_3$ (bold in Table 1) are $\geq$0.93.

If [2-^{13}C]-glucose is used as the carbon source both Glu and Pro generate singlet $^{13}C^{\beta}$ signals ($\geq$95% isolation), Fig. 3b and Table 1, and although Gln and Arg are not present in the Abp1p SH3 domain they are also expected to produce singlets since they derive from the same

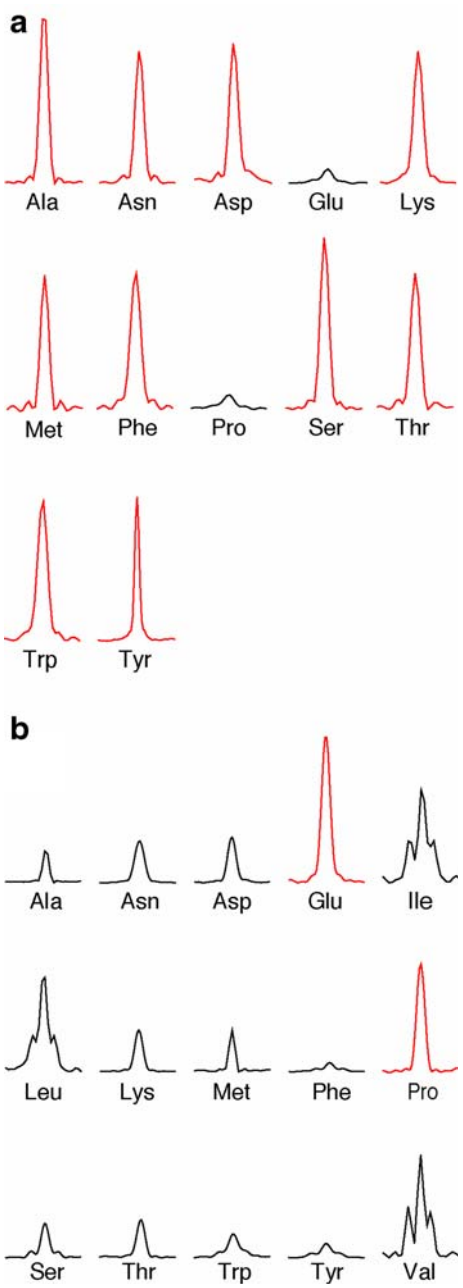

Fig. 3 $^{13}C^{\beta}$ traces from ^{13}C–^{1}H correlation maps showing observed multiplet patterns for all residue types present in the Abp1p SH3 domain produced using the labeling schemes presented in Fig. 2. A 1.0-ppm region is shown in all cases. A singlet indicates an isolated ^{13}C enriched position whereas a doublet separated by 35–55 Hz corresponds to a ^{13}C–^{13}C spin-pair. More complicated patterns than the superposition of a singlet and a doublet were not observed. **a** Examples of $^{13}C^{\beta}$–$^{1}H^{\beta}$ correlations from all residue types (for which cross peaks could be detected) in a sample produced from expression in *BL21(DE3)*Δ*sdh* cells with [1-^{13}C]-glucose/NaH$^{12}CO_3$ as carbon sources. All residue types with near isolated $^{13}C^{\beta}$ positions (≥93%, Table 1) and for which enrichment levels >30% are obtained are indicated in *red*. **b** Examples of $^{13}C^{\beta}$-$^{1}H^{\beta}$ correlations of all residue types in a sample produced with [2-^{13}C]-glucose and grown in *BL21(DE3)*Δ*sdh* cells. Only residue types that are enriched to ≈30% or greater and that contain near isolated $^{13}C^{\beta}$ are indicated in *red*. All traces are scaled to indicate relative enrichment levels (Table 1); the scaling is based on the relative intensities of the singlet multiplet components (i.e., total enrichment × fraction isolated)

precursors as Gln and Arg. As expected, correlations from Ile, Leu and Val indicate that these residues contain equal populations of $^{13}C^{\beta}$–^{13}C and isolated $^{13}C^{\beta}$ fragments while Phe, Ser, Trp and Tyr, that can only be ^{13}C labeled at C^{β} by the pentose phosphate pathway (Voet and Voet 1995), are also enriched with ^{13}C label at both β and α (Ser, Trp) or γ (Phe, Tyr) positions. $^{13}C^{\beta}$–$^{1}H^{\beta}$ correlations from many of the remaining residue types are dominated by the singlet component consistent with isolated or near isolated $^{13}C^{\beta}$ spins but as indicated in Fig. 3b and Table 1 the extent of labeling is low.

In summary, the results from the analysis of the levels of ^{13}C incorporation and the extent of formation of isolated $^{13}C^{\beta}$ positions suggest that there are 11 residue types (Ala, Asn, Asp, Cys, Lys, Met, Phe, Ser, Thr, Trp, Tyr) available for study by relaxation dispersion in protein samples produced by over-expression in *BL21(DE3)*Δ*sdh* cells with [1-^{13}C]-glucose/NaH$^{12}CO_3$ as the carbon source (bold in Table 1). An additional 4 residues (Arg, Gln, Glu, Pro) emerge from samples produced using [2-^{13}C]-glucose as the carbon source (bold in Table 1) and in cases where sensitivity is not limiting Ala, Asn, Asp, Cys, Lys, Met, Thr may also be suitable although these residues are labeled at a much higher level by [1-^{13}C]-glucose. As a final note it is worth reiterating that it is also possible to express proteins using [1,3-^{13}C]-glycerol or [2-^{13}C]-glycerol with the Δ*sdh* cell strain to generate levels of $^{13}C^{\beta}$ enrichment that are twice those reported here for glucose, albeit at the expense of less protein production, at least in the case of the Abp1p SH3 domain that is the focus of this study. The choice of a glycerol- or glucose-based growth strategy depends on the relative levels of expression for the protein considered, as well as issues of cost since [1-^{13}C]-glucose is approximately three-fold cheaper than either of the glycerol precursors.

A pulse scheme for the measurement of relaxation dispersion profiles for $^{13}CH_2$ groups

Figure 4 shows the pulse sequence that has been developed for the measurement of ^{13}C relaxation dispersion profiles for isolated $^{13}CH_2$ moieties in proteins. The pulse scheme follows closely a similar experiment that was developed to quantify ^{15}N dispersions derived from $^{15}NH_2$ groups of Asn and Gln side-chains (Mulder et al.2001a, b). The flow of magnetization during the sequence is

$$^{1}H^{\beta} \rightarrow {}^{13}C^{\beta} \rightarrow \text{CPMG} \rightarrow {}^{13}C^{\beta}(t_1) \rightarrow {}^{1}H^{\beta}(t_2) \quad (1)$$

with the CPMG pulse-train split by an element that ensures that the effective ^{13}C transverse relaxation rate for the duration of the constant-time CPMG relaxation period is independent of the number of refocusing pulses (Loria et al. 1999; Mulder et al.2001a, b). We have chosen to use 'aliphatic' selective pulses for the pulse train so that $^{13}C^{\beta}$ magnetization derived from Asp/Asn residues with $^{13}C^{\beta}$–$^{13}C^{\gamma}$ pairs (corresponding to 7% of the total magnetization from these residues) would be refocused, just as for isolated spins.

The $^{13}C^{\beta}$ spin can, of course, be directly coupled to either one, two or three protons and separate pulse schemes must be employed depending on whether there are an odd or even number of coupling partners. For example, the pulse trains applied before and after the so-called P-element in the center of the CPMG train in Fig. 4 must have orthogonal phases for CH and CH_3 spin systems, but not for CH_2 moieties. Sequences for recording ^{13}C CPMG dispersion profiles for isolated ^{13}CH and $^{13}CH_3$ groups have been published previously (Hansen et al. 2008b; Lundström et al. 2007b) and we have used these sequences in the present study. As a final note it is worth emphasizing that purging elements that eliminate magnetization from coupled $^{13}C^{\beta}$–^{13}C spin-pairs (Mulder et al. 2002; Wand et al. 1995) were not employed in any of the pulse schemes used in the present study. Typically these schemes are on the order of $1/(2J_{CC}) \approx 15$ ms in duration and for applications involving even small proteins relaxation losses during this interval can be considerable. For the 15 residues with near isolated $^{13}C^{\beta}$ spins (see above) purging is not necessary; in some cases the small contributions to the signal that arise from the approximately 5% of C^{β} carbons that are one bond homonuclear scalar coupled can be minimized by restricting measurement of peak intensities to regions focused on the singlet component. Accurate dispersion profiles for quantification of exchange involving $^{13}C^{\beta}$ probes from Ile, Leu or Val require measurement using versions of the experiments that include purge elements and this has not been done in the present study.

Experimental verification

The labeling scheme described above leads to reasonably high levels of $^{13}C^{\beta}$ enrichment (30–40%) for 15 of the 19 amino acids as well as minimal contamination by scalar coupled $^{13}C^{\beta}$–^{13}C spin-pairs. For systems that do not undergo chemical exchange it is expected that $^{13}C^{\beta}$ $R_{2,\mathrm{eff}}(\nu_{\mathrm{CPMG}})$ values measured for these residues would therefore be independent of the repetition rate of refocusing pulses (i.e., that flat dispersion curves would be obtained). By contrast, for residues such as Ile, Leu and Val, where a large fraction of the $^{13}C^{\beta}$ labeling is in the form of coupled ^{13}C–^{13}C spins, the evolution of magnetization due to homonuclear scalar couplings produces significant artifacts in dispersion curves. By recording dispersion profiles in a non-exchanging system it is possible to evaluate the extent of artifacts that are produced by scalar couplings and to get a qualitative feel for whether it might be possible to measure accurate $^{13}C^{\beta}$ chemical shifts. As a first control we have recorded dispersion profiles for a sample of the Abp1p SH3 domain produced with [1-^{13}C]-glucose. Because there is very little chemical exchange in the apo version of this protein (flat dispersion profiles for backbone spin-probes in the apo state) (Vallurupalli et al. 2008a, b; Hansen et al. 2008a, b; Lundström et al. 2009) it is expected that the 11 residue types produced from 3PG, PEP, pyruvate and OA will generate flat dispersion profiles. This can be quantified by calculating

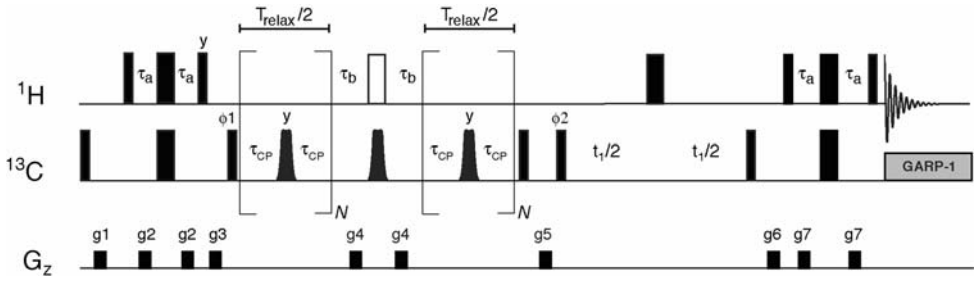

Fig. 4 Pulse sequence for the measurement of $^{13}C^{\beta}$ CPMG relaxation dispersion profiles of 'isolated' $^{13}C^{\beta}H_2$ groups in proteins. ^{1}H and ^{13}C 90° (180°) pulses are shown as *narrow (wide) bars*. The ^{1}H carrier is placed on the water signal, while the ^{13}C carrier is at 38 ppm. The ^{1}H pulse in the middle of the constant-time CPMG relaxation delay (duration T_{relax}) is of the composite $90°_x$–$180°_y$–$90°_x$ variety (Levitt 1986), while the shaped ^{13}C refocusing pulses have profiles very similar to those of RE-BURP pulses (Geen and Freeman 1991) so as not to perturb any small residual labeling of ^{13}CO of side chains. A detained description of the pulses is supplied in Lundström et al. (2008) with the major difference a flatter refocusing profile than for RE-BURPs. N is even. A so-called P-element (Loria et al. 1999; Mulder et al. 2001a,, b) is applied in the center of the CPMG element so that the effective $^{13}C^{\beta}$ transverse relaxation rates are independent of N. ^{13}C decoupling during acquisition is achieved using a 2–2.5 kHz GARP-1 field (Shaka et al. 1985). The delays τ_a and τ_b are set to 1.6 and 1.85 ms, respectively and the phase cycle is $\phi_1 = x, -x$, $\phi_2 = 2(x), 2(-x)$, receiver = x, 2(−x), x. Quadrature detection in t_1 is achieved via States-TPPI of $\varphi 2$ (Marion et al. 1989)

$$\mathrm{RMSD} = \sqrt{\mathrm{ND}^{-1}\sum_i \left\{R^i_{2,\mathrm{eff}}(\nu_{\mathrm{CPMG},i}) - k\right\}^2}$$

where $R^i_{2,\mathrm{eff}}$is the effective transverse relaxation rate at CPMG frequency $\nu_{\mathrm{CPMG},i}$, $k = \langle R_{2,\mathrm{eff}}(\nu_{\mathrm{CPMG}})\rangle$ and ND is the number of data points in the dispersion profile. RMSD values of 1.03 ± 0.34 s^{-1} are calculated that are higher than values obtained previously for labeling at other sites (average values of 0.12 s^{-1} of 0.5 s^{-1} for ^{15}N and ^{1}H$^{\alpha}$), but still reasonably small (see below).

As a second step, we wanted to establish that accurate values of $^{13}C^{\beta}$ chemical shift differences could be extracted from fits of relaxation dispersion profiles. For this purpose an exchanging system was used that has been described previously, based on the binding reaction:

$$\mathrm{P} + \mathrm{L} \underset{k_{\mathrm{off}}}{\overset{k_{\mathrm{on}}}{\rightleftharpoons}} \mathrm{PL}, \quad \mathrm{K_D} = 0.55 \pm 0.05\ \mu\mathrm{M} \qquad (2)$$

where P is the Abp1p SH3 domain and L a 17 residue peptide from the protein Ark1p. If only a small fraction L is added (5–10%), apo P remains the visible, ground state while PL is the invisible, 'excited' state. Since the exchange rate constant is on the order of several hundreds per second when

$$\frac{[\mathrm{PL}]}{[\mathrm{P}] + [\mathrm{PL}]} \approx 5 - 10\%,$$

25°C, well within the window of CPMG relaxation dispersion experiments, the chemical shift differences between probes in P and PL can be extracted from fits of dispersion profiles. These values can subsequently be compared with those obtained directly from measurements of peak positions in samples of P (apo SH3 domain) and PL (SH3 domain with saturating amounts of Ark1p peptide). As described in the section 'Materials and methods' samples were prepared with

$$\frac{[\mathrm{PL}]}{[\mathrm{P}] + [\mathrm{PL}]} \approx 12\%$$

([1-^{13}C]-glucose) and

$$\frac{[\mathrm{PL}]}{[\mathrm{P}] + [\mathrm{PL}]} \approx 4\%$$

([2-^{13}C]-glucose) and the pulse scheme of Fig. 4 was used to record $^{13}C^{\beta}$ dispersion profiles for all residue types with $^{13}C^{\beta}H_2$ groups, with additional profiles for Ala ($^{13}C^{\beta}H_3$) and Thr ($^{13}C^{\beta}H$) obtained from measurements on the 12%, [1-^{13}C]-glucose sample using previously published pulse sequences (Hansen et al. 2008b; Lundström et al. 2007b).

Dispersion profiles were initially selected for analysis based on the F-test criterion discussed in the section 'Materials and methods'. Notably, a significant number of clearly artifactual, very small and 'noisy' dispersion profiles with $\Delta R_{2,\mathrm{eff}} \leq 2$ s^{-1} were retained at this step that arise from $^{13}C^{\beta}$–^{13}C couplings that modulate the echoes produced during the CPMG pulse train. Indeed, in a previous study focusing on ^{13}C-methyl dispersion measurements in T4 lysozyme (labeled using $^{13}CH_3$-pyruvate) we noted small dispersion profiles for Leu residues that were clearly far removed from the site of exchange, resulting from three-bond $^{13}C^{\alpha}$–$^{13}C^{\delta}$ couplings (Mulder et al. 2002). We have also observed a similar situation in measurements of $^{13}C^{\alpha}$ dispersion profiles where many of the non-exchanging sites show profiles with $\Delta R_{2,\mathrm{eff}} = 1$–$2$ s^{-1} (Hansen et al. 2008b). In order to ensure that 'contamination' from this artifact is minimal in studies here, we have selected only those residues for which $\Delta R_{2,\mathrm{eff}} \geq 5$ s^{-1} (800 MHz) for further analysis (but see below).

Figure 5 illustrates a number of $^{13}C^{\beta}$ dispersion profiles (open circles) measured on samples prepared with either [1-^{13}C]-glucose, $p_B \approx 12\%$ (a) or [2-^{13}C]-glucose, $p_B \approx 4\%$ (b). Dispersion curves from each sample were fitted simultaneously to obtain global parameters k_{ex} and p_B as well as the residue specific parameters $|\Delta\varpi|$ and $R_{2,o}$. The global exchange values so obtained for the [1-^{13}C]-glucose, $p_B \approx 12\%$ sample, $k_{ex} = 330 \pm 30$ s^{-1} and $p_B = 12 \pm 0.8\%$, based on analysis of 14 dispersion profiles (10 residues) were consistent with those measured from analysis of an ^{15}N relaxation dispersion experiment that was recorded initially. In the case of labeling with [2-^{13}C]-glucose, fewer high quality dispersion profiles were obtained since only the four AKG-derived residues are enriched to high levels with isolated $^{13}C^{\beta}$ spins and regrettably two of the four (Arg, Gln) are not present in the Abp1p SH3 domain. We have therefore used dispersion profiles from other residues that are enriched to levels of approximately 10% at C^{β} and where the C^{β} position is isolated (Asn, Asp, Lys, see Table 1) that not surprisingly were of lower quality than those derived from amino acids with enrichment levels of 30–40%. Seven dispersion profiles (from 4 residues) were fitted using k_{ex} and p_B values obtained from ^{15}N data and $|\Delta\varpi|$ values extracted. Signs of $|\Delta\varpi|$ and hence the chemical shifts of the excited state could be obtained by measuring peak positions in HMQC- and HSQC-type datasets recorded at a number of static magnetic fields (Skrynnikov et al. 2002), although we have not done so here.

The accuracy of $^{13}C^{\beta}$ $|\Delta\varpi|$ values extracted from fits of dispersion profiles is established by comparison with shift differences that are measured directly on fully bound and free Abp1p SH3 domains. Figure 6 shows a comparison of $|\Delta\varpi_{\mathrm{CPMG}}|$ (*Y*-axis) and $|\Delta\varpi_{\mathrm{Direct}}|$ for samples produced using [1-^{13}C]-glucose/NaH$^{12}CO_3$ (a) or [2-^{13}C]-glucose (b) as carbon sources. The pair-wise RMSD between the CPMG/Direct datasets is 0.16 ppm (a) and 0.27 ppm (b). An obvious outlier in both correlation plots is $|\Delta\varpi|$ from Asn53, that deviates by 0.42 and 0.50 ppm (average of fits

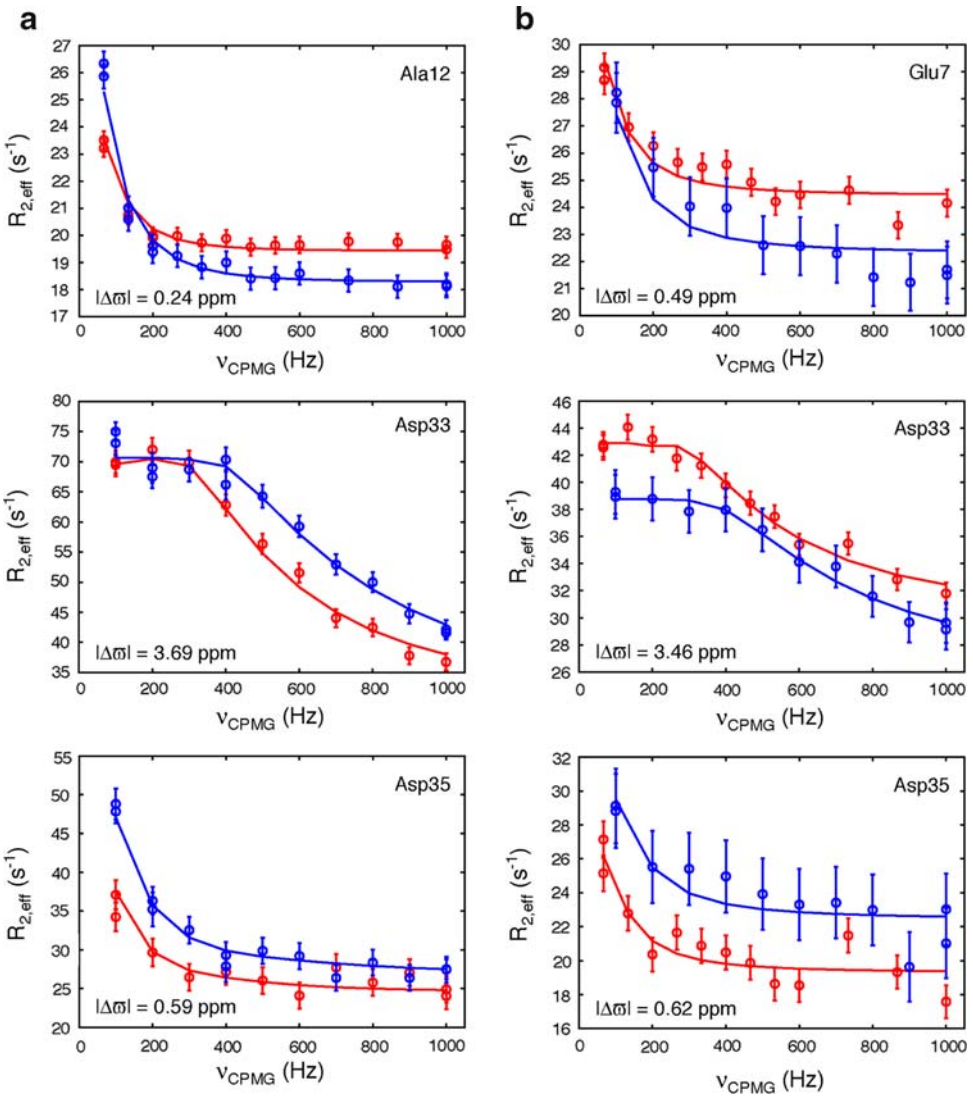

Fig. 5 Examples of $^{13}C^{\beta}$ relaxation dispersion profiles recorded on the fractionally bound Abp1p SH3 domain-Ark1p peptide complex, 25°C, with the SH3 domain over-expressed in *BL21(DE3)Δsdh* cells using [1-^{13}C]-glucose/NaH$^{12}CO_3$ or [2-^{13}C]-glucose as carbon sources. *Blue* and *red* symbols denote data recorded at 800 and 600 MHz, respectively, the *vertical lines* are error bars calculated on the basis of repeat measurements and the *solid lines* are fits to a global two-state model of chemical exchange. Fitted absolute values of the differences in chemical shifts between the free (ground) and bound (excited) Abp1p SH3 domain states are indicated. **a** $^{13}C^{\beta}$ dispersion profiles for 12% Ark1p peptide bound to the Abp1p SH3 domain produced using [1-^{13}C]-glucose/NaH$^{12}CO_3$. The data for Ala12 in the *upper panel* was recorded using a previously published pulse sequence designed for methyl groups (Lundström et al. 2007b) while the data in the *bottom two panels* were recorded with the pulse scheme presented in Fig. 4. **b** $^{13}C^{\beta}$ dispersions measured on a sample with 4% Ark1p peptide bound to the Abp1p SH3 domain produced using [2-^{13}C]-glucose. Data for all residues was recorded using the pulse sequence of Fig. 4

from profiles derived from the two $^{13}C^{\beta}$–$^{1}H^{\beta}$ correlations) from the expected value. Because the same trend is observed from both samples and almost identical values of $|\Delta\varpi|$ were calculated directly from peak positions in three different bound and free samples, we are convinced that differences in sample conditions are not the reason for the discrepancy and currently the origin of this difference is unknown. Shown in the insets to each of the figures are log-scale plots of $|\Delta\varpi_{CPMG}|$ versus $|\Delta\varpi_{Direct}|$ that are obtained from fits of dispersion data that satisfy the F-test criterion for selection, irrespective of $\Delta R_{2,eff}$. It is clear that $|\Delta\varpi|$ values are overestimated by the CPMG method for $|\Delta\varpi| \leq 0.2$ ppm. Most important, however, is that even if these 'false positive dispersions' are included in the analysis they are fit to small $|\Delta\varpi|$ values that would not lead to errors in predicted secondary structure elements nor in estimated (Φ, Ψ) values based on data base analyses (Cornilescu et al. 1999). In this regard it is worth noting that the accuracy of predicted $^{13}C^{\beta}$ chemical shifts using the best current algorithm, SPARTA, is 1.07 ppm (Shen and Bax 2007), well

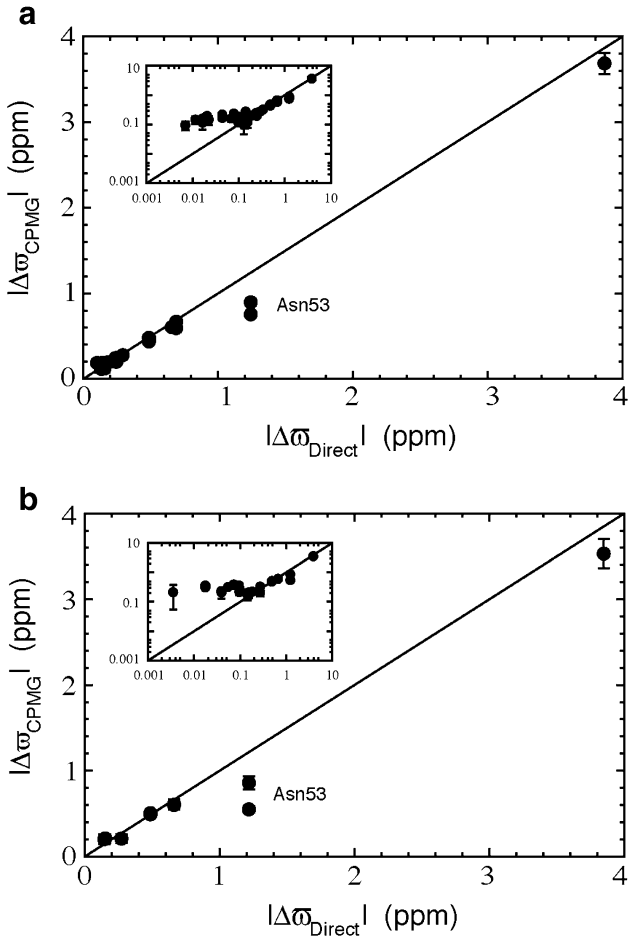

Fig. 6 Correlation between $^{13}C^{\beta}$ $|\Delta\varpi|$ values (ppm) extracted from fits of relaxation dispersion data recorded on samples of selectively labeled, fractionally bound Abp1p SH3 domains (*Y*-axis) and $^{13}C^{\beta}$ $|\Delta\varpi|$ values measured from peak positions in spectra of free and fully bound Abp1p SH3 domains (*X*-axis). Only data from fits of dispersion profiles that 'pass' the F-test criterion discussed in the section 'Materials and methods' and for which $\Delta R_{2,\mathrm{eff}} \geq 5\ \mathrm{s}^{-1}$ (800 MHz) were included. Shown in the insets are log-log plots of $|\Delta\varpi|$ values from fits of residues irrespective of $\Delta R_{2,\mathrm{eff}}$. **a** and **b** show data from the samples produced by over-expression in *BL21(DE3)*Δ*sdh* cells using [1-^{13}C]-glucose/NaH$^{12}CO_3$ and [2-^{13}C]-glucose as carbon sources respectively. For some residues with well resolved $^{1}H^{\beta}$ peaks it is possible to measure dispersions from both of the $^{13}C^{\beta}$–$^{1}H^{\beta}$ correlations; in these cases $|\Delta\varpi|$ values from separate fits of each dispersion curve are shown (for example, Asn53)

below the accuracy that can be measured via relaxation dispersion so that measurements of $^{13}C^{\beta}$ $|\Delta\varpi|$ values will be very useful as restraints in structural characterization of protein excited states. Of course, the accuracy of extracted $^{13}C^{\beta}$ $|\Delta\varpi|$ values will likely decrease as intrinsic relaxation rates of $^{13}C^{\beta}$ increase. Applications to medium sized proteins may benefit from a strategy in which $^{13}C^{\beta}HD$ moieties are produced by over-expression of protein in a mixture of H_2O/D_2O as was currently described in an application involving the use of glycine $^{13}C^{\alpha}$ spins as probes of exchange (Vallurupalli et al. 2009).

In summary, we have established a labeling scheme that produces isolated, reasonably highly ^{13}C enriched C^{β} positions in proteins that surpasses what can be achieved with random fractional labeling. In the application considered here samples are produced by over-expression in a commonly used bacterial strain with a single lesion in the TCA cycle using either [1-^{13}C]-glucose/NaH$^{12}CO_3$ or [2-^{13}C]-glucose as carbon sources. Proteins can also be expressed in this strain using suitably labeled glycerol precursors (LeMaster and Kushlan 1996), leading to a factor of two increased enrichment at $^{13}C^{\beta}$ over the levels reported for glucose in the present study, although often at the expense of smaller protein yields. Proteins produced with the labeling profile described are advantageous for the measurement of relaxation properties in studies of ps-ns time-scale dynamics, for example, where the generation of isolated ^{13}C positions simplifies the number of spin-interactions that must be considered (LeMaster and Kushlan 1996). Additionally such samples have found utility in solid-state NMR applications where they are produced in wild-type *E. coli* cell lines (Castellani et al. 2002; Wasmer et al. 2008). Use of the BL21(*DE3*)*Δsdh* cell line will lead to 'cleaner' samples in the sense that there will be fewer ^{13}C–^{13}C spin-pairs, an important consideration in the solid-state NMR work as well, without compromising the level of protein expression. However, a major utility of these samples is for the measurement of $^{13}C^{\beta}$ chemical shifts in invisible, excited protein states. Herein we have shown that accurate $^{13}C^{\beta}$ shifts can be obtained via relaxation dispersion measurements. As such the present work extends the dispersion methodology and provides yet another in a growing list of experiments for characterizing biologically important, yet short-lived and low populated conformers.

Acknowledgments We thank Dr. Jack Greenblatt, University of Toronto, for the gift of plasmids used for the knockout of succinate dehydrogenase and for valuable advice regarding this procedure. P. Vallurupalli and D. F. Hansen are thanked for useful discussion. This research was supported by a grant from The Canadian Institutes of Health Research. PL is supported by The Swedish Research Council. LEK holds a Canadian Research Chair in Biochemistry.

References

Boehr DD, McElheny D, Dyson HJ, Wright PE (2006) The dynamic energy landscape of dihydrofolate reductase catalysis. Science 313:1638–1642

Bystrov VF (1976) Spin-spin coupling and the conformational states of peptide systems. Prog Nucl Mag Res Spectrosc 10:41–82

Carr HY, Purcell EM (1954) Effects of diffusion on free precession in nuclear magnetic resonance experiments. Phys Rev 94:630–638

Castellani F, van Rossum B, Diehl A, Schubert M, Rehbein K, Oschkinat H (2002) Structure of a protein determined by solid-state magic-angle-spinning NMR spectroscopy. Nature 420:98–102

Cornilescu G, Delaglio F, Bax A (1999) Protein backbone angle restraints from searching a database for chemical shift and sequence homology. J Biomol NMR 13:289–302

Cronan JE, LaPorte DC (1996) Tricarboxylic cycle and glyoxylate bypass. In: Neidhardt FC, Curtiss R (eds) Escherichia coli and Salmonella: cellular and molecular biology. ASM Press, Washington D.C., pp 206–216

Datsenko KA, Wanner BL (2000) One-step inactivation of chromosomal genes in *Escherichia coli* K-12 using PCR products. Proc Natl Acad Sci USA 97:6640–6645

Delaglio F, Grzesiek S, Vuister GW, Zhu G, Pfeifer J, Bax A (1995) NMRPipe—a multidimensional spectral processing system based on unix pipes. J Biomol NMR 6:277–293

Drubin DG, Mulholland J, Zhu ZM, Botstein D (1990) Homology of a yeast actin-binding protein to signal transduction proteins and myosin-I. Nature 343:288–290

Eisenmesser EZ, Bosco DA, Akke M, Kern D (2002) Enzyme dynamics during catalysis. Science 295:1520–1523

Eisenmesser EZ, Millet O, Labeikovsky W, Korzhnev DM, Wolf-Watz M, Bosco DA, Skalicky JJ, Kay LE, Kern D (2005) Intrinsic dynamics of an enzyme underlies catalysis. Nature 438:117–121

Farmer BT, Venters RA (1999) NMR of perdeuterated larger proteins. In: Krishna NR, Berliner LJ (eds) Biological magnetic resonance, vol 16. Kluwer Academic/Plenum Publishers, New York, pp 75–120

Freeman R (1999) Spin choreography—basic steps in high resolution NMR. Oxford University Press, Oxford, p 123

Gardner KH, Kay LE (1998) The use of ^{2}H, ^{13}C, ^{15}N multidimensional NMR to study the structure and dynamics of proteins. Annu Rev Biophys Biomol Struct 27:357–406

Geen H, Freeman R (1991) Band-selective radiofrequency pulses. J Magn Reson 93:93–141

Goto NK, Gardner KH, Mueller GA, Willis RC, Kay LE (1999) A robust and cost-effective method for the production of Val, Leu, Ile (δ1) methyl-protonated ^{15}N-, ^{13}C-, ^{2}H-labeled proteins. J Biomol NMR 13:369–374

Gronostajski RM, Sadowski PD (1985) The Flp protein of the 2-micron plasmid of yeast—intermolecular and intramolecular reactions. J Biol Chem 260:2328–2335

Gross JD, Gelev VM, Wagner G (2003) A sensitive and robust method for obtaining intermolecular NOEs between side chains in large protein complexes. J Biomol NMR 25:235–242

Grzesiek S, Anglister J, Ren H, Bax A (1993) ^{13}C line narrowing by ^{2}H decoupling in $^{2}H/^{13}C/^{15}N$-enriched proteins—application to triple-resonance 4D J-connectivity of sequential amides. J Am Chem Soc 115:4369–4370

Hahn EL, Maxwell DE (1952) Spin echo measurements of nuclear spin coupling in molecules. Phys Rev 88:1070–1084

Hansen DF, Vallurupalli P, Kay LE (2008a) Quantifying two-bond ^{1}HN-^{13}CO and one-bond $^{1}H^{\alpha}$-$^{13}C^{\alpha}$ dipolar couplings of invisible protein states by spin-state selective relaxation dispersion NMR spectroscopy. J Am Chem Soc 130:8397–8405

Hansen DF, Vallurupalli P, Lundström P, Neudecker P, Kay LE (2008b) Probing chemical shifts of invisible states of proteins with relaxation dispersion NMR spectroscopy: how well can we do? J Am Chem Soc 130:2667–2675

Haynes J, Garcia B, Stollar EJ, Rath A, Andrews BJ, Davidson AR (2007) The biologically relevant targets and binding affinity requirements for the function of the yeast actin-binding protein 1 Src-homology 3 domain vary with genetic context. Genetics 176:193–208

Hill RB, Bracken C, DeGrado WF, Palmer AG (2000) Molecular motions and protein folding: characterization of the backbone dynamics and folding equilibrium of α_2D using ^{13}C NMR spin relaxation. J Am Chem Soc 122:11610–11619

Igumenova TI, Brath U, Akke M, Palmer AG (2007) Characterization of chemical exchange using residual dipolar coupling. J Am Chem Soc 129:13396–13397

Ikura M, Bax A (1992) Isotope-filtered 2D NMR of a protein peptide complex—study of a skeletal-muscle myosin light chain kinase fragment bound to calmodulin. J Am Chem Soc 114:2433–2440

Ishima R, Torchia DA (2003) Extending the range of amide proton relaxation dispersion experiments in proteins using a constant-time relaxation-compensated CPMG approach. J Biomol NMR 25:243–248

Ishima R, Baber J, Louis JM, Torchia DA (2004) Carbonyl carbon transverse relaxation dispersion measurements and ms-μs time-scale motion in a protein hydrogen bond network. J Biomol NMR 29:187–198

Kainosho M, Torizawa T, Iwashita Y, Terauchi T, Ono AM, Guntert P (2006) Optimal isotope labelling for NMR protein structure determinations. Nature 440:52–57

Kay LE, Torchia DA, Bax A (1989) Backbone dynamics of proteins as studied by ^{15}N inverse detected heteronuclear NMR-spectroscopy—application to staphylococcal nuclease. Biochemistry 28:8972–8979

Kay LE, Clore GM, Bax A, Gronenborn AM (1990a) 4-Dimensional heteronuclear triple-resonance NMR spectroscopy of interleukin-1-beta in solution. Science 249:411–414

Kay LE, Ikura M, Tschudin R, Bax A (1990b) 3-Dimensional triple-resonance NMR spectroscopy of isotopically enriched proteins. J Magn Reson 89:496–514

Korzhnev DM, Salvatella X, Vendruscolo M, Di Nardo AA, Davidson AR, Dobson CM, Kay LE (2004) Low-populated folding intermediates of Fyn SH3 characterized by relaxation dispersion NMR. Nature 430:586–590

Korzhnev DM, Neudecker P, Mittermaier A, Orekhov VY, Kay LE (2005) Multiple-site exchange in proteins studied with a suite of six NMR relaxation dispersion experiments: an application to the folding of a Fyn SH3 domain mutant. J Am Chem Soc 127:15602–15611

Lee LK, Rance M, Chazin WJ, Palmer AG (1997) Rotational diffusion anisotropy of proteins from simultaneous analysis of N-15 and C-13(alpha) nuclear spin relaxation. J Biomol NMR 9:287–298

LeMaster DM (1990) Deuterium labeling in NMR structural analysis of larger proteins. Q Rev Biophys 23:133–174

LeMaster DM, Kushlan DM (1996) Dynamical mapping of *E. coli* thioredoxin via ^{13}C NMR relaxation analysis. J Am Chem Soc 118:9255–9264

Levitt MH (1986) Composite pulses. Prog Nucl Mag Res Spectrosc 18:61–122

Li M, Ho PY, Yao SJ, Shimizu K (2006) Effect of sucA or sucC gene knockout on the metabolism in Escherichia coli based on gene expressions, enzyme activities, intracellular metabolite concentrations and metabolic fluxes by C-13-labeling experiments. Biochem Eng J 30:286–296

Lila T, Drubin DG (1997) Evidence for physical and functional interactions among two Saccharomyces cerevisiae SH3 domain proteins, an adenylyl cyclase-associated protein and the actin cytoskeleton. Mol Biol Cell 8:367–385

Löhr F, Rüterjans H (1998) Detection of nitrogen-nitrogen J-couplings in proteins. J Magn Reson 132:130–137

Loria JP, Rance M, Palmer AG (1999) A relaxation-compensated Carr-Purcell-Meiboom-Gill sequence for characterizing chemical exchange by NMR spectroscopy. J Am Chem Soc 121:2331–2332

Lundström P, Teilum K, Carstensen T, Bezsonova I, Wiesner S, Hansen DF, Religa TL, Akke M, Kay LE (2007a) Fractional 13C enrichment of isolated carbons using [1–13C]- or [2–13C]-glucose facilitates the accurate measurement of dynamics at backbone Ca and side-chain methyl positions in proteins. J Biomol NMR 38:199–212

Lundström P, Vallurupalli P, Religa TL, Dahlquist FW, Kay LE (2007b) A single-quantum methyl ^{13}C-relaxation dispersion experiment with improved sensitivity. J Biomol NMR 38:79–88

Lundström P, Hansen DF, Kay LE (2008) Measurement of carbonyl chemical shifts of excited protein states by relaxation dispersion NMR spectroscopy: comparison between uniformly and selectively ^{13}C labeled samples. J Biomol NMR 42:35–47

Lundström P, Hansen DF, Vallurupalli P, Kay LE (2009) Accurate measurement of alpha proton chemical shifts of excited protein states by relaxation dispersion NMR spectroscopy. J Am Chem Soc 131:1915–1926

Marion D, Ikura M, Tschudin R, Bax A (1989) Rapid recording of 2D NMR-spectra without phase cycling—application to the study of hydrogen-exchange in proteins. J Magn Reson 85:393–399

Meiboom S, Gill D (1958) Modified spin-echo method for measuring nuclear relaxation times. Rev Sci Instrum 29:688–691

Molenaar D, Van der Rest ME, Petrovic S (1998) Biochemical and genetic characterization of the membrane-associated malate dehydrogenase (acceptor) from *Corynebacterium glutamicum*. Eur J Biochem 254:395–403

Montelione GT, Wagner G (1990) Conformation-independent sequential NMR connections in isotope-enriched polypeptides by ^{1}H–^{13}C–^{15}N triple-resonance experiments. J Magn Reson 87:183–188

Mulder FAA, Mittermaier A, Hon B, Dahlquist FW, Kay LE (2001a) Studying excited states of proteins by NMR spectroscopy. Nat Struct Biol 8:932–935

Mulder FAA, Skrynnikov NR, Hon B, Dahlquist FW, Kay LE (2001b) Measurement of slow (μs-ms) time scale dynamics in protein side chains by ^{15}N relaxation dispersion NMR spectroscopy: application to Asn and Gln residues in a cavity mutant of T4 lysozyme. J Am Chem Soc 123:967–975

Mulder FAA, Hon B, Mittermaier A, Dahlquist FW, Kay LE (2002) Slow internal dynamics in proteins: application of NMR relaxation dispersion spectroscopy to methyl groups in a cavity mutant of T4 lysozyme. J Am Chem Soc 124:1443–1451

Palmer AG, Kroenke CD, Loria JP (2001) Nuclear magnetic resonance methods for quantifying microsecond-to-millisecond motions in biological macromolecules. Methods Enzymol 339:204–238

Palmer AG, Grey MJ, Wang CY (2005) Solution NMR spin relaxation methods for characterizing chemical exchange in high-molecular-weight systems. Methods Enzymol 394:430–465

Press WH, Flannery BP, Teukolsky SA and Vetterling WT (1988) Numerical recipes in C. University Press, Cambridge

Rath A, Davidson AR (2000) The design of a hyperstable mutant of the Abp1p SH3 domain by sequence alignment analysis. Protein Sci 9:2457–2469

Sattler M, Schleucher J, Griesinger C (1999) Heteronuclear multidimensional NMR experiments for the structure determination of proteins in solution employing pulsed field gradients. Prog Nucl Mag Res Spectrosc 34:93–158

Shaka AJ, Barker PB, Freeman R (1985) Computer-optimized decoupling scheme for wideband applications and low-level operation. J Magn Reson 64:547–552

Shen Y, Bax A (2007) Protein backbone chemical shifts predicted from searching a database for torsion angle and sequence homology. J Biomol NMR 38:289–302

Skrynnikov NR, Dahlquist FW, Kay LE (2002) Reconstructing NMR spectra of "invisible" excited protein states using HSQC and HMQC experiments. J Am Chem Soc 124:12352–12360

Spera S, Bax A (1991) Empirical correlation between protein backbone conformation and C^{α} and C^{β}–^{13}C nuclear magnetic resonance chemical shifts. J Am Chem Soc 113:5490–5492

Studier FW, Moffatt BA (1986) Use of bacteriophage-T7 RNA-polymerase to direct selective high-level expression of cloned genes. J Mol Biol 189:113–130

Sugase K, Dyson HJ, Wright PE (2007) Mechanism of coupled folding and binding of an intrinsically disordered protein. Nature 447:1021–1025

Tollinger M, Skrynnikov NR, Mulder FAA, Forman-Kay JD, Kay LE (2001) Slow dynamics in folded and unfolded states of an SH3 domain. J Am Chem Soc 123:11341–11352

Tugarinov V, Kay LE (2004) An isotope labeling strategy for methyl TROSY spectroscopy. J Biomol NMR 28:165–172

Vallurupalli P, Kay LE (2006) Complementarity of ensemble and single-molecule measures of protein motion: a relaxation dispersion NMR study of an enzyme complex. Proc Natl Acad Sci USA 103:11910–11915

Vallurupalli P, Hansen DF, Stollar E, Meirovitch E, Kay LE (2007) Measurement of bond vector orientations in invisible excited states of proteins. Proc Natl Acad Sci USA 104:18473–18477

Vallurupalli P, Hansen DF, Kay LE (2008a) Probing structure in invisible protein states with anisotropic NMR chemical shifts. J Am Chem Soc 130:2734–2735

Vallurupalli P, Hansen DF, Kay LE (2008b) Structures of invisible, excited protein states by relaxation dispersion NMR spectroscopy. Proc Natl Acad Sci USA 105:11766–11771

Vallurupalli P, Hansen DF, Lundström P, Kay LE (2009) CPMG relaxation dispersion NMR experiments measuring glycine $^{1}H^{\alpha}$ and $^{13}C^{\alpha}$ chemical shifts in the 'invisible' excited states of proteins. J Biomol NMR. doi 10.1007/s10858-009-9310-6

Voet D, Voet JG (1995) Biochemistry. Wiley, Hoboken

Wand AJ, Bieber RJ, Urbauer JL, McEvoy RP, Gan ZH (1995) Carbon relaxation in randomly fractionally ^{13}C-enriched proteins. J Magn Reson B 108:173–175

Wasmer C, Lange A, Van Melckebeke H, Siemer AB, Riek R, Meier BH (2008) Amyloid fibrils of the HET-s (218–289) prion form a beta solenoid with a triangular hydrophobic core. Science 319:1523–1526

Watt ED, Shimada H, Kovrigin EL, Loria JP (2007) The mechanism of rate-limiting motions in enzyme function. Proc Natl Acad Sci USA 104:11981–11986

Wishart DS, Case DA (2002) Use of chemical shifts in macromolecular structure determination. Methods Enzymol 338:3–34

Wishart DS, Sykes BD (1994) The ^{13}C chemical-shift index—a simple method for the identification of protein secondary structure using ^{13}C chemical-shift data. J Biomol NMR 4:171–180

Wolf-Watz M, Thai V, Henzler-Wildman K, Hadjipavlou G, Eisenmesser EZ, Kern D (2004) Linkage between dynamics and catalysis in a thermophilic-mesophilic enzyme pair. Nat Struct Mol Biol 11:945–949

Zeeb M, Balbach J (2005) NMR spectroscopic characterization of millisecond protein folding by transverse relaxation dispersion measurements. J Am Chem Soc 127:13207–13212

Zuiderweg ERP, Petros AM, Fesik SW, Olejniczak ET (1991) 4-Dimensional [^{13}C, ^{1}H, ^{13}C, ^{1}H] HMQC-NOE-HMQC NMR-spectroscopy—resolving tertiary NOE distance constraints in the spectra of larger proteins. J Am Chem Soc 113:370–372